nature photonics

Article

https://doi.org/10.1038/s41566-024-01566-0

Terawatt-attosecond hard X-ray free-electron laser at high repetition rate

Received: 27 May 2024

Accepted: 10 October 2024

Published online: 25 November 2024

Check for updates

Jiawei Yan[1] ✉, Weilun Qin[2], Ye Chen[2], Winfried Decking[2], Philipp Dijkstal[2,5], Marc Guetg[2], Ichiro Inoue[3,4], Naresh Kujala[1], Shan Liu[2], Tianyun Long[2], Najmeh Mirian[2] & Gianluca Geloni[1]

Ångstrom and attosecond are the fundamental spatiotemporal scales for electron dynamics in various materials. Although attosecond pulses with wavelengths comparable to the atomic scales are expected to be a key tool in advancing attosecond science, producing high-power hard X-ray attosecond pulses at ångstrom wavelengths remains a formidable challenge. Here, we report the generation of terawatt-scale attosecond hard X-ray pulses using a free-electron laser in a special operation mode. We achieved 9 keV single-spike X-ray pulses with a mean pulse energy of around 180 μJ, exceeding previous reports by more than an order of magnitude, and an estimated average pulse duration of 200 as at full-width at half-maximum. Exploiting the unique capability of the European XFEL, which can deliver ten pulse trains per second with each containing hundreds of pulses at megahertz repetition rates, this study demonstrates the generation of attosecond X-ray pulses at a 2.25 MHz repetition rate. These intense high-repetition-rate attosecond X-ray pulses present transformative prospects for structural and electronic damage-free X-ray measurements and attosecond time-resolved X-ray methodologies, heralding a new era in ultrafast X-ray science.

Since the discovery of X-rays in 1895, scientists have continuously endeavoured to increase the brilliance of X-ray sources to facilitate X-ray techniques, such as atomic-scale structure determination of matter by diffraction measurement, characterization of electronic structures in complex compounds by spectroscopy, and three-dimensional visualization of opaque samples by imaging techniques[1]. The recent advent and development of hard X-ray free-electron lasers (FELs)[2–6] has opened up unprecedented opportunities for X-ray science. The working principle of X-ray FELs[7,8] lies in the strong interaction between an electromagnetic field and a relativistic electron beam within an undulator consisting of a sequence of periodic dipole magnetic fields. Predominantly, modern X-ray FEL facilities worldwide utilize self-amplified spontaneous emission (SASE) to generate femtosecond X-ray pulses with gigawatt peak power[9]. This process exponentially amplifies radiation from electron beam shot noise through an undulator, achieving peak power levels several orders of magnitude higher than those of synchrotron radiation and tabletop X-ray sources.

The short pulse duration of hard X-ray FELs enables capturing signals from a sample before notable X-ray-induced changes in atomic configurations. This concept, often termed 'measurement-before-destruction'[10,11], opens a path for X-ray analysis of radiation-sensitive samples and environments, such as protein crystals at biologically relevant temperatures[12–14]. One remaining challenge for measurements with X-ray FELs is mitigating electronic damage. When an X-ray pulse irradiates matter, a large number of electrons are excited via a cascade of collisional ionization, triggered by the emission of photoelectrons and Auger electrons[15,16]. Since typical timescale of the electron excitation is a few femtoseconds[17–19], these excitations are not negligible when using femtosecond X-ray pulses for experiments. In fact, severe electronic damage in samples during X-ray FEL

[1]European XFEL, Schenefeld, Germany. [2]Deutsches Elektronen-Synchrotron DESY, Hamburg, Germany. [3]RIKEN SPring-8 Center, Hyogo, Japan. [4]University of Hamburg, CFEL, Hamburg, Germany. [5]Present address: Paul Scherrer Institut, Villigen, Switzerland. ✉e-mail: jiawei.yan@xfel.eu

https://doi.org/10.1038/s41566-024-01566-0

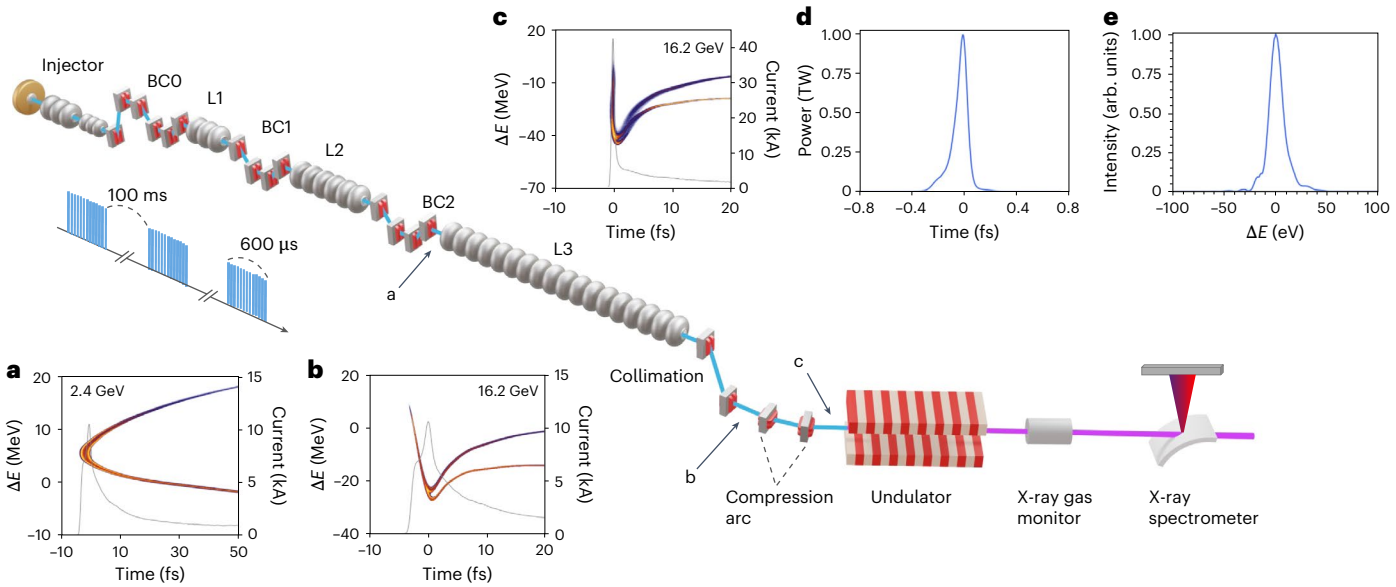

Fig. 1 | Schematic representation of the self-chirping operation mode at the European XFEL. The layout includes a photocathode electron gun, a 1.3 GHz superconducting booster, a 3.9 GHz third harmonic linearizer, a laser heater (not shown), three bunch compressors (BC0, BC1 and BC2), three superconducting linac sections (L1, L2 and L3), a collimation section and an arc section for transporting the electron beam to the SASE2 undulator. The European XFEL offers the ability to deliver ten bursts (trains) of electron beams every second. Each train is characterized by its flexibility in the number of electron bunches it contains, which can vary from a single bunch to a maximum of 2,700 bunches. The generated X-ray pulse, shown in purple, is analysed by the X-ray gas monitor[66,67] and the HIREX single-shot spectrometer[68], both depicted in grey and situated downstream from the undulator. **a**–**c**, Simulated longitudinal phase spaces of the electron beam at the exits of BC2 (**a**), the collimation section (**b**) and the arc section (**c**), with the beam head to the left. **d**,**e**, Simulated XFEL performance at 9 keV including the temporal profile (**d**) with an FWHM duration of around 110 as and a peak power of 1 TW and the corresponding spectrum (**e**) with an FWHM bandwidth of about 16 eV.

pulse irradiation has been reported in diffraction[20–22] and spectroscopy experiments[23,24].

The use of high-power sub-femtosecond hard X-ray pulses with 10^{11} to 10^{12} photons per pulse holds the promise of truly (structural and electronic) damage-free measurement, greatly enhancing the capabilities of measurements with X-ray FEL pulses. One intriguing topic is the structure determination of single protein molecules. To determine the orientation of these tiny samples, one may need to use X-ray pulses with high photon densities on the order of 10^{20} photons per mm^2 (refs. 25,26). Although focusing femtosecond X-ray pulses from existing XFEL facilities using state-of-the-art X-ray optics[27] can satisfy this requirement for photon density, severe changes in atomic scattering factors owing to electron excitation[17,19] may hinder precise structure determination. Sub-femtosecond X-ray pulses will pave the way for atomic-scale X-ray imaging of protein molecules, which would be a breakthrough in structural biology. Another promising application of sub-femtosecond X-ray pulses is nonlinear spectroscopy. Femtosecond X-ray FEL pulses now provide opportunities to access nonlinear processes involving multiple incident X-ray photons[28–32], which were not accessible with conventional X-ray sources. However, the application of nonlinear processes for material characterization has been quite limited[23,33] because X-ray intensity needs to be suppressed to the extent that electronic damage is negligible, resulting in small nonlinear signals. High-power sub-femtosecond pulses remove the limitation of X-ray intensity and allow efficient measurements of nonlinear signals.

Attosecond optical pulses have been generated by the high-harmonic generation process over the past two decades[34]. Although this technique can generate attosecond soft X-ray pulses[35–37], shortening the wavelengths to the hard X-ray region poses substantial difficulties owing to a marked decline in conversion efficiency with increasing photon energy. Meanwhile, there are continuous developments to shorten the duration of the XFEL pulse[9,38–40]. Multiple techniques are proposed to create an electron beam with a narrow current peak and generate a sub-femtosecond soft X-ray pulse[41–46]. In the hard X-ray regime, the generation of attosecond pulses is achieved through the use of electron bunches with reduced charge (tens of picocoulombs)[47–49] or electron bunches with a large transverse tilt[50]. The pulse energy of the attosecond pulses produced by these methods is a few to 10 µJ, which is more than two orders of magnitude lower than that of SASE XFEL pulses in normal operation, limiting the practical applications for the experiments. Furthermore, the attosecond XFEL has only been demonstrated at low repetition rates up to about 100 Hz. High-repetition-rate attosecond XFELs on the order of kilohertz to megahertz (MHz) will greatly shorten data collection time, offering substantial advantages for small cross-sectional experiments[51].

We here demonstrate the generation of high-power and high-repetition-rate attosecond hard X-ray pulses at the European XFEL[5,52]. The schematic layout of our experimental set-up, named self-chirping enabled attosecond X-ray pulse generation, is shown in Fig. 1. Figure 1a–e shows the simulated longitudinal phase spaces of the electron beam at different locations of the linear accelerator and the corresponding FEL performance. First, the relativistic electrons are accelerated in the off-peak phase of radio frequency (rf) structures to obtain an energy chirp along the electron beam. Then, we adjust the current distribution of the electron beam to form a ramped profile[47,53] with a prominent peak at the leading edge of the beam. This is achieved by controlling the phase and voltage of the high-harmonic rf structure before the bunch compressor, which longitudinally compresses the energy-chirped electron beam. As the beam passes through the linear accelerator after the last bunch compressor, the high current spike of the electron beam is energy modulated by the strong longitudinal space-charge field[54]. As a result, those electrons in the front portion of the high-current part gain energy and the back portion of the electrons lose energy, leading to the energy chirp in the high-current part of the electron beam. The energy chirp is further increased by the coherent radiation emitted by the electron beam when passing through bending

https://doi.org/10.1038/s41566-024-01566-0

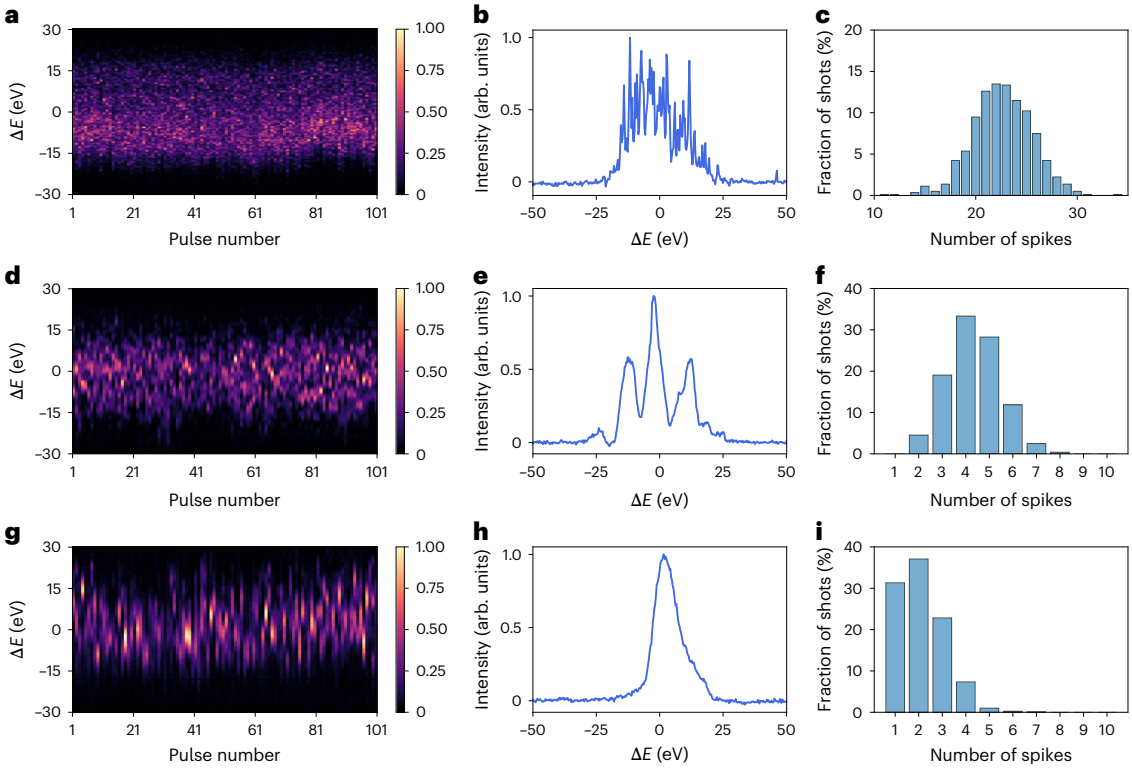

Fig. 2 | Spectral analysis under different operation modes. a–i, Spectral measurements and corresponding histograms for the number of spikes under the regular operation (**a**–**c**), after self-chirping (**d**–**f**) and arc compression (**g**–**i**) at a 10 Hz repetition rate. The left panels show 100 consecutive single-shot spectral measurements, the centre panels show a typical single-shot spectrum, and the right panels depict histograms based on 800 consecutive spectra.

dipole magnets[55,56]. We can further compress the electron beam with energy chirp induced by these self-chirping processes (energy modulation by space-charge and coherent synchrotron radiation effects) by using the arc section located before the undulator. The arc section was originally designed to deliver the electron beam to different undulator lines, and its longitudinal dispersion strength (R_{56}) can be controlled by tuning the quadrupoles inside. To compress the electron beam, the R_{56} of the arc section is set to a positive value, such that electrons of higher energy pass through the arc on longer trajectories than electrons of lower energy[57]. In addition, controlling the longitudinal dispersion within the arc simultaneously introduces transverse dispersion, which consequently imparts a transverse kick to the self-chirped electron beam. By controlling the orbit of the electron beam in the undulator, the high-peak current portion is kept on the axis for continuous FEL interaction, whereas the remaining portion of the beam undergoes consistent oscillation[58,59]. This helps to suppress radiation from the lower current parts of the beam and produces shorter XFEL pulses without side peaks.

Experiments were conducted at the SASE2 undulator line of the European XFEL utilizing an electron beam with a charge of 250 pC and an energy of 16.2 GeV. Figure 2a,b shows 100 consecutive measurements and a single representative spectrum of XFEL pulses generated at 9 keV under standard SASE operation with a repetition rate of 10 Hz. Figure 2c shows the histogram of the number of spikes, which are computed based on 800 consecutive spectra. The spectrum of the standard SASE pulse typically has more than 20 spikes. The mean pulse energy of the pulses, as measured by the X-ray gas monitor, is 2,170 ± 84 μJ. Figure 2d,e shows the measured spectra when the phase and voltage of the high-harmonic rf structure are optimized for the self-chirping process while the arc remains unchanged. Most of the XFEL pulses generated after self-chirping exhibit four or five spikes in the spectrum, as shown in Fig. 2f, with a measured pulse energy of 124 ± 26 μJ. These results indicate a reduction in XFEL pulse duration following the optimization of the high-harmonic rf structure. After optimization of R_{56} of the arc (R_{56} = 260 μm), most of the spectra have one or two SASE spikes (Fig. 2g–i); 31% (37%) of the pulses exhibit a single-spike (two-spike) spectrum. The measured pulse energy of all events is 174 ± 23 μJ.

We analysed 1,044 single-spike spectra out of 3,500 total consecutive spectra for the optimized condition of the arc. Figure 3a shows examples of spectra for XFEL pulses with a single spike. The shot-by-shot fluctuation of the pulse energy for the single-spike events is very small (Fig. 3b); the average and standard derivation of the pulse energy is 184 μJ and 22 μJ, respectively. Remarkably, over 90% of these single-spike pulses exhibit pulse energy exceeding 150 μJ. The histogram of the spectral width (full-width at half-maximum (FWHM)) of the single-spike events, which are computed based on the Gaussian fitting of the spectrum, is presented in Fig. 3c. The FWHM bandwidth for XFEL pulses with a single spike is 13.8 ± 3.4 eV. The bandwidth of the single-spike events is typically used to characterize the length of a hard X-ray FEL pulse in the temporal domain[44,47–49]. Assuming that these pulses follow Gaussian distributions constrained by the Fourier limit, the corresponding FWHM duration is 139 ± 37 as. Although the phase of the radiation pulse can lead to an underestimation of the duration of the XFEL pulses, the temporal duration of a hard X-ray FEL pulse can be estimated as a factor of $\sqrt{2}$ times its Fourier-limit duration[47], denoted as τ_f, assuming the pulse reaches the maximum possible absolute linear frequency chirp for a given spectral width (see Methods for details). When adopting this assumption, the duration of the single-spike events is estimated to be 197 ± 52 as, corresponding to an average peak power of around 0.9 TW. Figure 3d shows the pulse energy and $\sqrt{2}\tau_f$ of the single-spike events.

Since the self-chirping scheme depends only on the collective effects induced by the electron beam itself, it can be used to produce

https://doi.org/10.1038/s41566-024-01566-0

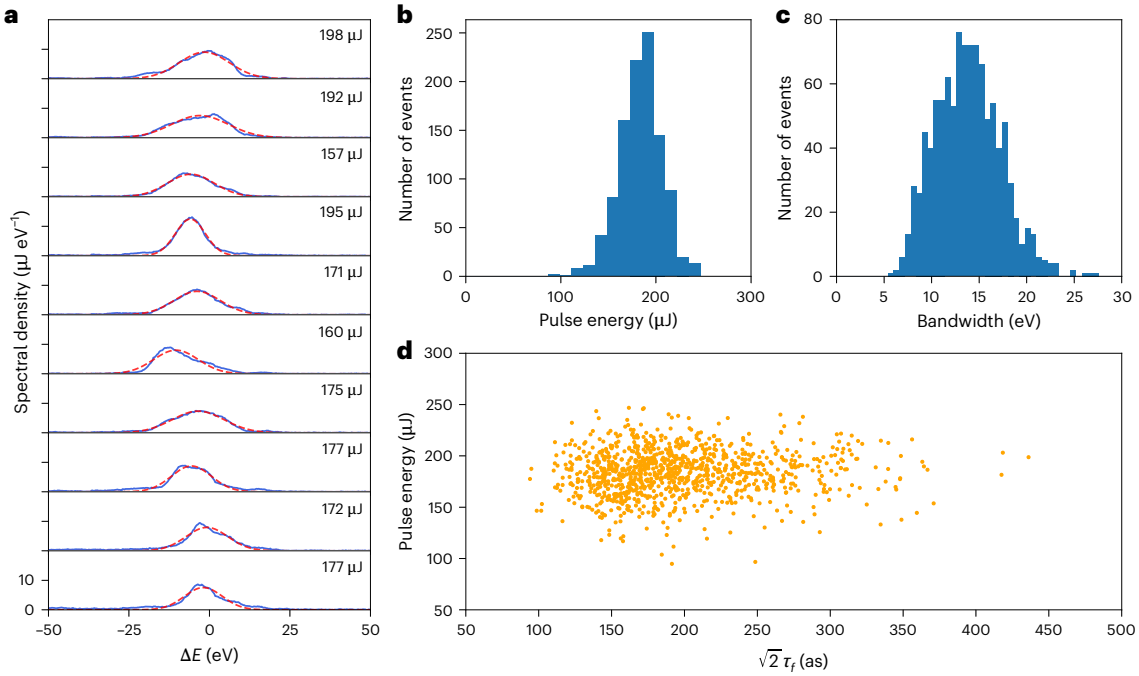

Fig. 3 | Analysis of single-spike spectra at 9 keV. a, Ten spectral measurements (solid lines) in the single-spike regime. Dashed lines indicate the corresponding Gaussian fits. **b**, Histogram representing the measured pulse energy from 1,044 recorded single-spike events. **c**, Histogram showcasing the FWHM bandwidths from these events. **d**, Scatter plot depicting the pulse energy against the estimation of pulse duration.

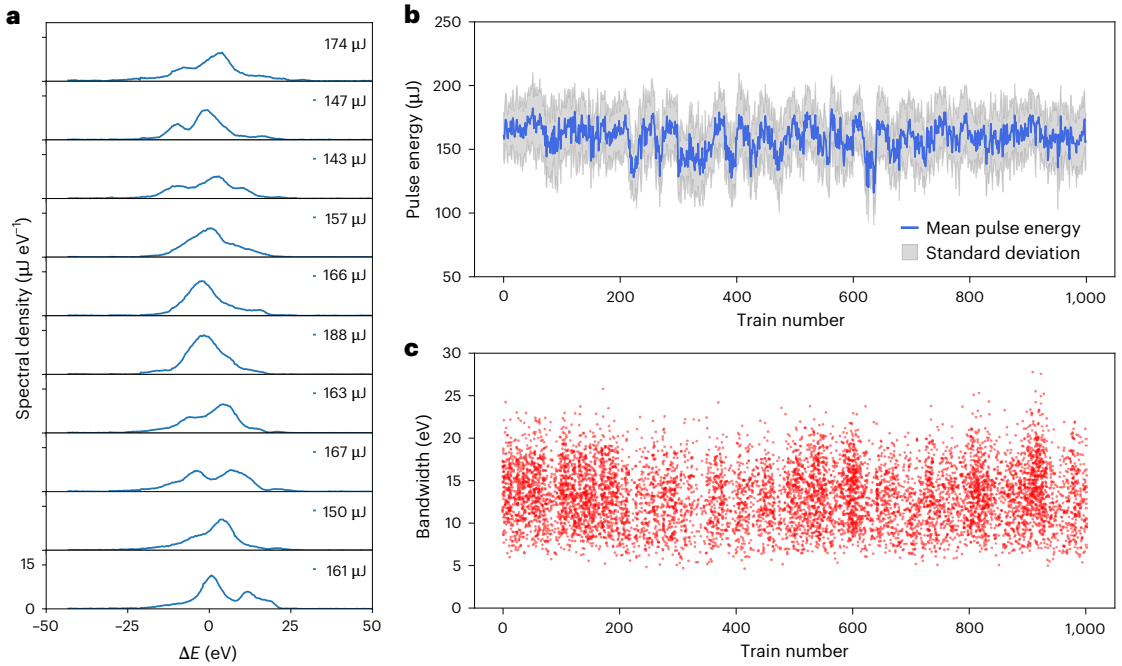

Fig. 4 | Performance of self-chirping operation mode at high repetition rate. a, Ten consecutive spectral measurements within a single train at an intra-train repetition rate of 2.25 MHz. **b**, Mean pulse energy of all events within a train as a function of train number. For each train, the mean pulse energy (solid line) and standard deviation (shaded area) are calculated from 200 pulses. **c**, FWHM bandwidth of the single-spike events as a function of train number.

high-repetition-rate attosecond X-ray pulses. Here, we demonstrated the feasibility of generating high-repetition-rate attosecond hard X-ray pulses by utilizing multi-bunch trains. Each train comprised 200 electron bunches at an intra-train repetition rate of 2.25 MHz, corresponding to a continuous average rate of 2 kHz. Figure 4 presents the high-repetition-rate performance of the self-chirping mode at a central photon energy of around 9 keV. At this working point, the high-resolution hard X-ray (HIREX) single-shot spectrometer samples the single-shot spectrum of every fourth pulse, resulting in a total of 50 spectra from each train. Figure 4a shows a sequence of ten consecutively sampled spectra within one pulse train. Figure 4b presents the distribution of pulse energies across 1,000 trains, with an average

measured pulse energy of 159 ± 26 μJ. Furthermore, Fig. 4c presents the measured bandwidth for those single-spike events across 1,000 pulse trains. The average bandwidth for all single-spike events is 13.3 ± 3.6 eV, corresponding to an estimated pulse duration of 207 ± 62 as. Spectral analysis of the 50,000 pulses (spanning 1,000 trains) indicates that 15% of the spectra are single spikes and 37% exhibited a two-spike structure. Compared with the pulses achieved at a 10 Hz repetition rate, the pulse energy and bandwidth of the high-repetition-rate pulses remained consistent, while the average number of spectrum spikes increased from 2.05 to 2.51. The observed increase in the average spectrum spikes is primarily attributed to imperfect trajectory correction along the pulse train[60]. Incorporating spectral quality into the orbit correction process is expected to enhance performance at high repetition rates further.

In summary, we have successfully generated single-spike X-ray pulses with energy levels in the hundreds of microjoules range at 9 keV photon energy. Our approach involves electron beam energy modulation through a self-chirping process in an accelerator driving the FEL, complemented by the application of an arc for further beam compression. The resulting single-spike XFEL pulses have an average duration at the 200 as level and an average pulse energy of 184 μJ. Moreover, we have demonstrated the generation of attosecond hard X-ray pulses at MHz repetition rates. The intensity of the hard X-ray attosecond pulse obtained in this experiment was more than an order of magnitude higher than previously reported at other hard X-ray FEL facilities, reaching 10^{11} photons per pulse. The high-intensity attosecond pulses with high stability and MHz repetition rate demonstrated in this study will open a door for various novel experimental techniques, such as atomic-scale X-ray imaging of protein molecules[10,61], nonlinear X-ray spectroscopy of functional materials[23,33], capturing attosecond electron motions in action[62,63] and demonstration of X-ray quantum imaging[64,65].

Online content

Any methods, additional references, Nature Portfolio reporting summaries, source data, extended data, supplementary information, acknowledgements, peer review information; details of author contributions and competing interests; and statements of data and code availability are available at https://doi.org/10.1038/s41566-024-01566-0.

References

1. Als-Nielsen, J. & McMorrow, D. *Elements of Modern X-ray Physics* (Wiley, 2011).
2. Emma, P. et al. First lasing and operation of an ångstrom-wavelength free-electron laser. *Nat. Photon.* **4**, 641–647 (2010).
3. Ishikawa, T. et al. A compact X-ray free-electron laser emitting in the sub-ångström region. *Nat. Photon.* **6**, 540–544 (2012).
4. Kang, H.-S. et al. Hard X-ray free-electron laser with femtosecond-scale timing jitter. *Nat. Photon.* **11**, 708–713 (2017).
5. Decking, W. et al. A MHz-repetition-rate hard X-ray free-electron laser driven by a superconducting linear accelerator. *Nat. Photon.* **14**, 391–397 (2020).
6. Prat, E. et al. A compact and cost-effective hard X-ray free-electron laser driven by a high-brightness and low-energy electron beam. *Nat. Photon.* **14**, 748–754 (2020).
7. Huang, Z. & Kim, K.-J. Review of X-ray free-electron laser theory. *Phys. Rev. Spec. Top. Accel. Beams* **10**, 034801 (2007).
8. Pellegrini, C., Marinelli, A. & Reiche, S. The physics of X-ray free-electron lasers. *Rev. Mod. Phys.* **88**, 015006 (2016).
9. Huang, N., Deng, H., Liu, B., Wang, D. & Zhao, Z. Features and futures of X-ray free-electron lasers. *Innovation* **2**, 100097 (2021).
10. Neutze, R., Wouts, R., van der Spoel, D., Weckert, E. & Hajdu, J. Potential for biomolecular imaging with femtosecond X-ray pulses. *Nature* **406**, 752–757 (2000).
11. Chapman, H. N., Caleman, C. & Timneanu, N. Diffraction before destruction. *Phil. Trans. R. Soc. B* **369**, 20130313 (2014).
12. Chapman, H. N. et al. Femtosecond X-ray protein nanocrystallography. *Nature* **470**, 73–77 (2011).
13. Boutet, S. et al. High-resolution protein structure determination by serial femtosecond crystallography. *Science* **337**, 362–364 (2012).
14. Bostedt, C. et al. Linac coherent light source: the first five years. *Rev. Mod. Phys.* **88**, 015007 (2016).
15. Ziaja, B., van der Spoel, D., Szöke, A. & Hajdu, J. Auger-electron cascades in diamond and amorphous carbon. *Phys. Rev. B* **64**, 214104– (2001).
16. Ziaja, B., London, R. A. & Hajdu, J. Unified model of secondary electron cascades in diamond. *J. Appl. Phys.* **97**, 064905 (2005).
17. Son, S.-K. et al. Impact of hollow-atom formation on coherent X-ray scattering at high intensity. *Phys. Rev. A* **83**, 033402 (2011).
18. Hau-Riege, S. P. Photoelectron dynamics in X-ray free-electron-laser diffractive imaging of biological samples. *Phys. Rev. Lett.* **108**, 238101 (2012).
19. Fratalocchi, A. & Ruocco, G. Single-molecule imaging with X-ray free-electron lasers: dream or reality? *Phys. Rev. Lett.* **106**, 105504 (2011).
20. Nass, K. et al. Indications of radiation damage in ferredoxin microcrystals using high-intensity X-FEL beams. *J. Synchrotron Radiat.* **22**, 225–238 (2015).
21. Inoue, I. et al. Atomic-scale visualization of ultrafast bond breaking in X-ray-excited diamond. *Phys. Rev. Lett.* **126**, 117403 (2021).
22. Inoue, I. et al. Femtosecond reduction of atomic scattering factors triggered by intense X-ray pulse. *Phys. Rev. Lett.* **131**, 163201 (2023).
23. Tamasaku, K. et al. Nonlinear spectroscopy with X-ray two-photon absorption in metallic copper. *Phys. Rev. Lett.* **121**, 083901 (2018).
24. Alonso-Mori, R. et al. Femtosecond electronic structure response to high intensity XFEL pulses probed by iron X-ray emission spectroscopy. *Sci. Rep.* **10**, 16837 (2020).
25. Shneerson, V. L., Ourmazd, A. & Saldin, D. K. Crystallography without crystals. I. The common-line method for assembling a three-dimensional diffraction volume from single-particle scattering. *Acta Crystallogr. A* **64**, 303–315 (2008).
26. Fung, R., Shneerson, V., Saldin, D. K. & Ourmazd, A. Structure from fleeting illumination of faint spinning objects in flight. *Nat. Phys.* **5**, 64–67 (2009).
27. Yamada, J. et al. Extreme focusing of hard X-ray free-electron laser pulses enables 7 nm focus width and 10^{22} W cm^{-2} intensity. *Nat. Photon.* **18**, 685–690 (2024).
28. Shwartz, S. et al. X-ray second harmonic generation. *Phys. Rev. Lett.* **112**, 163901 (2014).
29. Tamasaku, K. et al. X-ray two-photon absorption competing against single and sequential multiphoton processes. *Nat. Photon.* **8**, 313–316 (2014).
30. Fuchs, M. et al. Anomalous nonlinear X-ray Compton scattering. *Nat. Phys.* **11**, 964–970 (2015).
31. Yoneda, H. et al. Saturable absorption of intense hard X-rays in iron. *Nat. Commun.* **5**, 5080 (2014).
32. Yoneda, H. et al. Atomic inner-shell laser at 1.5-ångström wavelength pumped by an X-ray free-electron laser. *Nature* **524**, 446–449 (2015).
33. Tamasaku, K. et al. Two-dimensional Kβ-Kα fluorescence spectrum by nonlinear resonant inelastic X-ray scattering. *Nat. Commun.* **14**, 4262 (2023).
34. Krausz, F. & Ivanov, M. Attosecond physics. *Rev. Mod. Phys.* **81**, 163 (2009).
35. Silva, F., Teichmann, S. M., Cousin, S. L., Hemmer, M. & Biegert, J. Spatiotemporal isolation of attosecond soft X-ray pulses in the water window. *Nat. Commun.* **6**, 6611 (2015).

36. Li, J. et al. 53-attosecond X-ray pulses reach the carbon K-edge. *Nat. Commun.* **8**, 186 (2017).
37. Johnson, A. S., Avni, T., Larsen, E. W., Austin, D. R. & Marangos, J. P. Attosecond soft X-ray high harmonic generation. *Phil. Trans. R. Soc. A* **377**, 20170468 (2019).
38. Zholents, A. A. Method of an enhanced self-amplified spontaneous emission for X-ray free electron lasers. *Phys. Rev. Spec. Top. Accel. Beams* **8**, 040701 (2005).
39. Saldin, E. L., Schneidmiller, E. A. & Yurkov, M. V. Self-amplified spontaneous emission FEL with energy-chirped electron beam and its application for generation of attosecond X-ray pulses. *Phys. Rev. Spec. Top. Accel. Beams* **9**, 050702 (2006).
40. Parc, Y. W., Shim, C. H. & Kim, D. E. Toward the generation of an isolated TW-attosecond X-ray pulse in XFEL. *Appl. Sci.* **8**, 1588 (2018).
41. Duris, J. et al. Tunable isolated attosecond X-ray pulses with gigawatt peak power from a free-electron laser. *Nat. Photon.* **14**, 30–36 (2020).
42. Zhang, Z. et al. Experimental demonstration of enhanced self-amplified spontaneous emission by photocathode temporal shaping and self-compression in a magnetic wiggler. *New J. Phys.* **22**, 083030 (2020).
43. Funke, L. et al. Capturing nonlinear electron dynamics with fully characterised attosecond X-ray pulses. Preprint at https://arxiv.org/abs/2408.03858 (2024).
44. Prat, E. et al. Coherent sub-femtosecond soft X-ray free-electron laser pulses with nonlinear compression. *APL Photon.* **8**, 111302 (2023).
45. Li, S. et al. 'Beam a la carte': laser heater shaping for attosecond pulses in a multiplexed X-ray free-electron laser. Preprint at https://arxiv.org/abs/2404.02299 (2024).
46. Franz, P. et al. Terawatt-scale attosecond X-ray pulses from a cascaded superradiant free-electron laser. *Nat. Photon.* **18**, 698–703 (2024).
47. Huang, S. et al. Generating single-spike hard X-ray pulses with nonlinear bunch compression in free-electron lasers. *Phys. Rev. Lett.* **119**, 154801 (2017).
48. Malyzhenkov, A. et al. Single- and two-color attosecond hard X-ray free-electron laser pulses with nonlinear compression. *Phys. Rev. Res.* **2**, 042018 (2020).
49. Marinelli, A. et al. Experimental demonstration of a single-spike hard-X-ray free-electron laser starting from noise. *Appl. Phys. Lett.* **111**, 151101 (2017).
50. Dijkstal, P. *Temporal FEL Pulse Shaping and Diagnostics at SwissFEL with Tilted Electron Beams*. PhD thesis, ETH Zurich (2022).
51. Tschentscher, T. Investigating ultrafast structural dynamics using high repetition rate X-ray FEL radiation at European XFEL. *Eur. Phys. J. Plus* **138**, 274 (2023).
52. Liu, S. et al. Cascaded hard X-ray self-seeded free-electron laser at megahertz repetition rate. *Nat. Photon.* **17**, 984–991 (2023).
53. Piot, P. et al. Generation and characterization of electron bunches with ramped current profiles in a dual-frequency superconducting linear accelerator. *Phys. Rev. Lett.* **108**, 034801 (2012).
54. Chao, A. W. *Physics of Collective Beam Instabilities in High Energy Accelerators* (Wiley Series in Beam Physics and Accelerator Technology, 1993).
55. Saldin, E. L., Schneidmiller, E. A. & Yurkov, M. On the coherent radiation of an electron bunch moving in an arc of a circle. *Nucl. Instrum. Methods Phys. Res. A* **398**, 373–394 (1997).
56. Balandin, V., Brinkmann, R., Decking, W. & Golubeva, N. Post-linac collimation system for the European XFEL. Preprint at https://arxiv.org/abs/1305.1544 (2013).
57. Schlarb, H. & Brinkmann, R. Ultra-short bunches by using a quasi-continuous compressor scheme in a long beam transfer line. In *Proc. 1997 Particle Accelerator Conference* 1572–1574 (IEEE, 1997).
58. Lutman, A. A. et al. Fresh-slice multicolour X-ray free-electron lasers. *Nat. Photon.* **10**, 745–750 (2016).
59. Guetg, M. W., Lutman, A. A., Ding, Y., Maxwell, T. J. & Huang, Z. Dispersion-based fresh-slice scheme for free-electron lasers. *Phys. Rev. Lett.* **120**, 264802 (2018).
60. Obier, F., Decking, W., Hüning, M. & Wortmann, J. Long pulse kicker for European XFEL beam distribution. In *Proc. 39th Free Electron Laser Conference* 357–359 (JACoW Publishing, 2019).
61. Miao, J., Ishikawa, T., Robinson, I. K. & Murnane, M. M. Beyond crystallography: diffractive imaging using coherent X-ray light sources. *Science* **348**, 530–535 (2015).
62. Yong, H., Sun, S., Gu, B. & Mukamel, S. Attosecond charge migration in molecules imaged by combined X-ray and electron diffraction. *J. Am. Chem. Soc.* **144**, 20710–20716 (2022).
63. Yong, H., Cavaletto, S. M. & Mukamel, S. Ultrafast valence-electron dynamics in oxazole monitored by X-ray diffraction following a stimulated X-ray Raman excitation. *J. Phys. Chem. Lett.* **12**, 9800–9806 (2021).
64. Schneider, R. et al. Quantum imaging with incoherently scattered light from a free-electron laser. *Nat. Phys.* **14**, 126–129 (2018).
65. Classen, A., Ayyer, K., Chapman, H. N., Röhlsberger, R. & von Zanthier, J. Incoherent diffractive imaging via intensity correlations of hard X rays. *Phys. Rev. Lett.* **119**, 053401 (2017).
66. Maltezopoulos, T. et al. Operation of X-ray gas monitors at the European XFEL. *J. Synchrotron Radiat.* **26**, 1045–1051 (2019).
67. Sorokin, A. A. et al. An X-ray gas monitor for free-electron lasers. *J. Synchrotron Radiat.* **26**, 1092–1100 (2019).
68. Kujala, N. et al. Hard X-ray single-shot spectrometer at the European X-ray free-electron laser. *Rev. Sci. Instrum.* **91**, 103101 (2020).

Methods

Simulation

The particle distribution with a charge of 250 pC and a beam energy of 6 MeV is generated using ASTRA[69]. Further acceleration, compression and electron beam transport are simulated using Ocelot[70]. At the entrance of the undulator, the electron beam energy is accelerated to 16.2 GeV and the FWHM width of the current spike is ~1 fs. The three-dimensional FEL simulation is performed with Genesis 1.3 (ref. 71). The FEL simulation with 500 random seeds shows that 22% of events exhibit a single frequency spike, while 53% present two frequency spikes. The FWHM bandwidth and pulse duration of the single frequency spike events are 14 ± 4.5 eV and 177 ± 79 as, respectively, indicating that the pulse duration is about 1.38 times the Fourier-transform limit. The average peak power of the single-spike events (all events) is 0.7 TW (0.75 TW).

X-ray spectrum diagnostics

The X-ray spectra were measured with the high-resolution hard X-ray single-shot spectrometer-II (HIREX-II spectrometer)[68], which is installed in the photon tunnel XTD6 of the SASE2 undulator line. Two detection systems are installed for train-to-train observations: the first one is an optical system for a low repetition rate of 10 Hz with a resolution of 0.2 eV px^{-1} using the Si(440) reflection, and the other contains a GOTTHARD detector[72] for MHz repetition rate to resolve pulses within trains with a resolution of around 0.3 eV px^{-1} using diamond C(220).

XFEL pulse duration estimation

The undulator magnetic field causes a forward slippage of the X-rays relative to the electrons. Together with the inherent stochastic nature of SASE, this leads to the formation of independent coherent radiation spikes[73]. The average spike length is given by the slippage over one gain length and is referred to as the cooperation length $l_c = \lambda_r \times L_g/\lambda_u$, where λ_r is the radiation wavelength, L_g is the gain length and λ_u is the undulator period. Assuming a linear chirped Gaussian pulse with a given bandwidth and frequency chirp, there are two possible solutions for its duration[47]:

$$\tau_p = \frac{2\sqrt{2\ln 2/\pi}}{\sqrt{\Delta f_p^2 \pm \sqrt{\Delta f_p^4 - \left(4\ln 2\alpha f_0/\pi\right)^2}}} \quad (1)$$

where Δf_p is the FWHM frequency width, f_0 is the central frequency and α is the frequency chirp parameter. While f_0 and Δf_p can be measured, α can only be estimated either from FEL simulations or from the empirically optimized undulator taper value[49]. When $|\alpha| = \pi\Delta f_p^2/(4\ln 2 f_0)$, representing the maximum achievable absolute frequency chirp for a specific spectral width and central frequency, both solutions of equation (1) are equal to $\sqrt{2}\tau_f$, where τ_f is the transform-limited pulse duration. For smaller $|\alpha|$, two distinct solutions are obtained, one smaller and one larger than $\sqrt{2}\tau_f$. On the basis of FEL simulations, it is possible to exclude the larger solution. The peak power of the pulse can be estimated using the expression $0.94 \times E_p/\tau_p$, where E_p is the pulse energy.

Data availability

The data that support the plots in Figs. 1–4 are available via figshare at https://doi.org/10.6084/m9.figshare.27068008 (ref. 74). All other data used in this study are available from the corresponding author on reasonable request.

References

69. Floettmann, K. Astra: a space charge tracking algorithm. http://www.desy.de/~mpyflo/ (1997).
70. Agapov, I., Geloni, G., Tomin, S. & Zagorodnov, I. Ocelot: a software framework for synchrotron light source and FEL studies. *Nucl. Instrum. Methods Phys. Res. A* **768**, 151–156 (2014).
71. Reiche, S. Genesis 1.3: a fully 3D time-dependent FEL simulation code. *Nucl. Instrum. Methods Phys. Res. A* **429**, 243–248 (1999).
72. Mozzanica, A. et al. The GOTTHARD charge integrating readout detector: design and characterization. *J. Instrum.* **7**, C01019 (2012).
73. Bonifacio, R., De Salvo, L., Pierini, P., Piovella, N. & Pellegrini, C. Spectrum, temporal structure and fluctuations in a high-gain free-electron laser starting from noise. *Phys. Rev. Lett.* **73**, 70 (1994).
74. Yan, J. et al. Dataset for 'Terawatt-attosecond hard X-ray free-electron laser at high repetition rate'. *figshare* https://doi.org/10.6084/m9.figshare.27068008 (2024).

Acknowledgements

We thank H. Chapman, H. Deng, J. E, T. Feurer, J. Liu, C. Lechner, S. Molodtsov, A. Madsen, S. Serkez, M. Scholz and Z. Zhu for many fruitful discussions and for their interest in this work. J.Y. extends special thanks to J. Huang from UMass Amherst for insightful discussions on protein structures and dynamics. This work was supported by the computational resources of the Maxwell at Deutsches Elektronen-Synchrotron (DESY), Hamburg, Germany.

Author contributions

J.Y. conceived and led the experiment, conducted data analysis and simulation, and wrote the paper draft. W.Q. conducted the longitudinal phase space measurement, machine set-up and data analysis, and participated in the experiment. Y.C. led the electron beam dynamics simulation and participated in the experiment. W.D. participated in the experimental activities and contributed to the coordination of the experimental activities. P.D. contributed to the experimental data analysis. M.G. participated in the experimental activities and contributed to the coordination of the experimental activities. I.I. contributed to the experimental activities and discussion on potential scientific applications. N.K. contributed to the spectrum measurement. T.L. conducted the spectral data analysis and FEL simulation, and participated in the experiment. S.L. contributed to the spectral data analysis and participated in the experiment. N.M. participated in the experimental activities. G.G. participated in the experiment and contributed to the coordination of the experimental activities. All authors co-wrote the paper.

Funding

Open access funding provided by Deutsches Elektronen-Synchrotron (DESY).

Competing interests

The authors declare no competing interests.

Additional information

Supplementary information The online version contains supplementary material available at https://doi.org/10.1038/s41566-024-01566-0.

Correspondence and requests for materials should be addressed to Jiawei Yan.

Peer review information *Nature Photonics* thanks David Attwood, Heung-Sik Kang and the other, anonymous, reviewer(s) for their contribution to the peer review of this work.